J Multidisciplinary Scientific Journal

MDPI

Review

Direct Photon Production in High-Energy Heavy Ion Collisions within the Integrated Hydrokinetic Model

Yuri Sinyukov * and Volodymyr Shapoval

Department of High-Density Energy Physics, Bogolyubov Institute for Theoretical Physics, 03143 Kyiv, Ukraine; shapoval@bitp.kiev.ua
* Correspondence: sinyukov@bitp.kiev.ua

Abstract: The results on description of direct photon yields, transverse momentum spectra, and flow harmonics, measured in ultrarelativistic heavy-ion collisions at the Relativistic Heavy Ion Collider (RHIC) and the Large Hadron Collider (LHC) for different collision centrality classes, analyzed within the Integrated Hydrokinetic Model (iHKM) are reviewed. The iHKM simulation results, corresponding to the two opposite approaches to the matter evolution treatment at the final stage of the system's expansion within the model, namely, the chemically equilibrated and the chemically frozen evolution, are compared. The so-called "direct photon puzzle" is addressed, and its possible solution, suggesting the account for additional photon emission at confinement, is considered.

Keywords: photon; spectrum; elliptic flow; triangular flow; RHIC; LHC

Citation: Sinyukov, Y.; Shapoval, V. Direct Photon Production in High-Energy Heavy Ion Collisions within the Integrated Hydrokinetic Model. *J* **2022**, *5*, 1–14. https://doi.org/10.3390/j5010001

Academic Editor: Astrid Morreale

Received: 29 November 2021
Accepted: 4 January 2022
Published: 6 January 2022

1. Introduction

The analysis of the experimental data on high-energy nucleus-nucleus collisions allows one to conclude that a new form of strongly interacting matter, extremely hot and dense one, is formed in these processes. It is believed that quarks and gluons in this new state of matter are not confined in hadrons, so that such a state is called Quark–Gluon Plasma (QGP). The experimental and theoretical study of QGP constitutes a major task for the present research programs in the field of high-density energy physics.

In particular, QGP is the only source of exotic particles, containing *strange*, or even heavier *charm* and *bottom*, quarks. These quarks are not included in protons and neutrons that make up usual matter we normally see around us. They can be produced only in deconfined state of matter created in relativistic A+A collisions, when high kinetic energy of colliding nuclei transforms, inter alia, into the mass of newly formed heavy quarks. The analysis of exotic particle yields, their ratios and other relevant observables measured in the experiments allow one to investigate the deep properties of QGP. On the other hand, the study of peculiarities of the Quark–Gluon matter evolution process and its eventual breakup into particles, as well as the development of realistic models of these processes facilitates the description and the interpretation of data related to the heavy flavor production.

The Integrated Hydrokinetic Model (iHKM) of high-energy heavy-ion collisions [1,2] repeatedly showed good results in simultaneous description/prediction of a variety of hadron bulk observables for different colliding nuclei at different relativistic energies [2–7]. These results particularly included the successful description of strange mesons (K, $K^*(892)$, $\phi(1020)$) and strange baryons (Λ, Ω, Ξ) production, as well as kaon and pion femtoscopy. Thus, one can say that more or less realistic picture of relativistic A+A collision was eventually constructed within the iHKM model. The aspect which was missing in this picture was the description of experimental data on photon production and solving the so-called "direct photon puzzle".

The latter task should be considered quite important, since photon radiation produced in relativistic heavy-ion collisions is a unique probe for exploring the properties of the created system and the dynamics of its evolution, since photons are emitted at all the stages

of the matter expansion and do not strongly interact with it, thus providing the undistorted information about the system's state at the moment of photon emission for each class of the produced photons [8–11].

All the photons radiated during the matter evolution are usually divided into *decay photons*, i.e., those coming from hadron decays (e.g., from π^0, ω, and η meson decays) [12], and *direct photons*, including all the other photons apart from the decay ones. The direct photons, in turn, are subdivided into *prompt photons*, i.e., the photons emitted at the very initial stage of the two nuclei collision as a result of hard partonic scatterings and jet fragmentations, *pre-equilibrium photons*, coming from the hot guark-gluon matter at the early stage of its evolution, while it has not yet reached a nearly thermal and locally-equilibrated state (this includes also the glasma phase [13–17]), and *thermal photons*, emitted from the expanding nearly thermalized continuous Quark–Gluon medium [18], as well as from the hadron-resonance gas formed at the late stage of the collision, when continuous QGP gets finally transformed into particles [19]. One can also consider such direct photon sources as jet-photon conversion and jet-induced bremsstrahlung [20,21], involving the interaction of hard partons with the thermal QGP medium.

The thermal direct photons are of particular interest, since they can give us an insight into spatio-temporal structure, collective flow and temperature of the evolving system (however, extraction of this information is somewhat complicated due to superposition of the contributions from different temporal stages of the matter evolution in the resulting spectrum). The thermal photons are dominant in the low-p_T part of the spectrum, where they form a nearly exponential p_T distribution. As for the prompt photons, they can help us test the correctness of perturbative Quantum ChromoDynamics (pQCD) calculations and investigate the parton distribution functions of the colliding nuclei. The prompt photons play a major role in high-p_T region of the spectrum, demonstrating a power law behavior.

Some time ago the experimental results on direct-photon production obtained for Au+Au collisions at the top RHIC energy, $\sqrt{s_{\rm NN}} = 200$ GeV, and for Pb+Pb collisions at the LHC energy $\sqrt{s_{\rm NN}} = 2.76$ TeV were presented in the articles by the PHENIX Collaboration [22–25] and the ALICE Collaboration [26–28], respectively. The results for both energies demonstrated a similar distinctive feature, namely, the unexpectedly large yields of thermal photons combined with the large elliptic flow v_2. The first attempts to describe such a peculiarity of the data within hydrodynamic/hybrid models did not succeed: the models either described the measured p_T spectra, but underestimated v_2, or they gave large enough v_2, however the corresponding photon yields were too low [16,29–32]. This motivated new intensive research activity aiming to solve the arisen "direct photon flow puzzle" [13,33–35].

In particular, additional mechanisms of direct photon production were proposed to be taken into account. For example, the photon yields can be increased due to the conformal anomaly in the presence of a very strong magnetic field created in non-central collisions [36,37] or due to synchrotron radiation [38,39]. One more mechanism, allowing to enhance direct-photon anisotropy is "magnetic bremsstrahlung-like radiation" of quarks in the collective color field ensuring confinement [40]. The other possible extra sources of photon radiation, associated with the confinement of QGP medium, are described in [41–44]. However, although these mechanisms look quite realistic from a theoretical point of view, accounting for them has not lead to fairly clear phenomenological predictions.

Recently, the analysis of direct-photon production in heavy-ion collisions at the mentioned RHIC and LHC energies, was also performed within the integrated hydrokinetic model [45,46]. The calculations of thermal photon emission within iHKM were carried out in the two different approaches to the description of the matter evolution at the post-hydrodynamic stage—the chemically equilibrated and the chemically frozen ones. A new possible contribution to the photon spectra connected with the hadronization process was also proposed aiming to improve the observables description and, if possible, to resolve the direct photon puzzle. In this review paper we summarize and re-examine the results obtained in the original works [45,46].

2. Photon Emission Sources

2.1. Prompt Photons

The prompt photons are radiated at the earliest stage of the nucleus-nucleus interaction. They are mainly produced in QCD Compton scattering and $q\bar{q}$ annihilation processes and, additionally, in processes of QCD jets fragmentation. Naturally, the corresponding γ spectra are calculated within the perturbative QCD. In order to obtain prompt photon spectra for A+A collision case, one can take into account the experimental results presented in References [47,48], which indicate that the prompt photon momentum spectra scale with the number of binary nucleon-nucleon collisions, N_{coll}. Thus, to calculate the spectra for Au+Au and Pb+Pb collisions one can rescale the pQCD result for $p+p$ collision case with the corresponding binary collision number N_{coll}, which can be estimated using a Monte Carlo Glauber approach [49].

Generally, the prompt photon production cross-section in $p+p$ collisions can be expressed as follows

$$d\sigma_{pp} = \sum_{i,j,k} f_i(x_i, Q_{fact}) \otimes f_j(x_j, Q_{fact}) \otimes d\hat{\sigma}_{ij\to k}(Q_{ren}) \otimes D_k^{\gamma}(x_k, Q_{frag}), \quad (1)$$

where the summation is performed over all the different processes of partonic interactions, producing prompt photons, f_i and f_j are parton distribution functions (PDFs), D_k^{γ} is the parton-to-photon fragmentation function and $d\hat{\sigma}$ is the corresponding partonic process cross-section. The latter is calculated based on the perturbative expansion with respect to the strong coupling constant, $\alpha_s(Q_{ren})$.

As one can see, in order to calculate the cross-section $d\sigma_{pp}$, one should specify the three QCD scales, Q_{fact}, Q_{ren}, and Q_{frag}, entering (1). In our consideration the values of all the three scales are fixed to $Q = 0.5\ p_T$, since it is commonly known that the smaller is the constant of proportionality between Q and p_T, the better data description can be reached.

To calculate the prompt γ transverse momentum spectra in case of proton-proton collisions we utilize the JETPHOX code [50]. At high photon p_T (perturbative region) one can use the optimal relation $Q = 0.5\ p_T$. However, one can face the problem, when applying the mentioned parametrization for relatively small photon momenta, $p_T < Q_0/\lambda$ GeV/c, where λ is the proportionality coefficient between Q and p_T, and $Q_0 \approx 1.5$ GeV/c is the energy-momentum scale usually considered as the limit of pQCD applicability. Fortunately, it can be shown that changing the λ value results simply in the renormalization of the photon spectrum [13]. So, the low-p_T part of the spectrum can be obtained by rescaling the spectrum, calculated at larger λ value, e.g., at $Q = 4\ p_T$, in accordance with the high-p_T results for the case of $Q = 0.5\ p_T$.

In our study, the EPS09 parton distribution function [51] and the BFG II fragmentation function [52] were used in tabular form for prompt photon spectra calculations.

2.2. Pre-Equilibrium and Thermal Photons

The pre-thermal and thermal photon contributions are treated in our consideration based on the matter evolution description, obtained within the iHKM model. The model simulates the full process of the evolution of the system formed in a high-energy nuclear collision, which can be divided into several stages, each described using a relevant approach (see our previous papers, e.g., [1,2,46] for a detailed model description).

The initial state at the proper time τ_0, serving a starting point for the subsequent pre-equilibrium energy-momentum tensor dynamics within a relaxation-time approximation [1,53], is modeled with the help of GLISSANDO code [54–56]. It gives us the initial energy-density transverse profile $\epsilon(\mathbf{r}_\mathrm{T})$, containing contributions from the binary collision and the wounded nucleon models, which is then scaled by the factor ϵ_0—iHKM parameter, characterizing the initial energy density in the center of the system. One more iHKM parameter, α defines the fraction of binary collisions in the resulting $\epsilon(\mathbf{r}_\mathrm{T})$ distribution. During the pre-thermal expansion system gradually equilibrates, so that before the thermalization

time $\tau_{\rm th} \approx 1$ fm/c, it becomes nearly thermal and thus can be further described within the viscous hydrodynamics approximation.

At the next, hydrodynamic stage the system expansion is described using the Israel–Stewart formalism with the Laine–Schroeder equation of state (EoS) for the Quark–Gluon matter [57]. We also use the minimal possible shear viscosity to entropy density ratio $\eta/s = 0.08 \approx 1/4\pi$ in our simulations. So, the system gradually cools down, and when the temperature reaches the particlization value, $T_p = 165$ MeV, one performs sharp switching to the description in terms of particles based on the Cooper–Frye prescription (the particlization hypersurface is constructed using the Cornelius routine [58]). Finally, the generated particles are forwarded to the UrQMD hadron cascade [59,60], which describes the afterburner stage of the system's evolution.

The last sentence corresponds to the original iHKM model used for the description of hadronic observables. However, the description of photon emission at the final stage of matter evolution presently cannot be explicitly implemented in UrQMD, so that we use two alternative approaches of γ radiation treatment at the post-hydrodynamic stage.

The first variant is to continue the hydrodynamic evolution of the hadron matter in a *chemically equilibrated* way until the photon radiation becomes negligible, e.g., until the temperature drops to the values lower than $T \approx 100$ MeV. In this case, one can determine the hydrodynamic velocities $u^\mu(x)$ and the temperatures $T(x)$ at the final stage of collision straightforwardly, so that the thermal photon production from the expanding hadronic medium can be easily calculated based on the well-known results for the emission of photons from a thermal hadronic system in rest. Such a method has a noticeable disadvantage, namely, the fact that at low enough temperatures (still relevant to the evolution of considered hadronic system) the chemical equilibrium gets definitely broken.

Another way of dealing with the afterburner stage suggests using the original version of hydrokinetic model—HKM [61]. The latter features *chemically frozen* matter evolution with continuous particlization, in course of which the local chemical equilibrium, as well as the local thermal one, are violated. The chemical composition of the expanding system does not change due to inelastic reactions, which are all switched off, except for the resonance decays. Such a picture of the late stage of the collision corresponds to the widespread conception of chemical freeze-out. It requires the introduction of separate chemical potential for each sort of hadron, thus complicating the simulation of the system's evolution as compared to the chemical equilibrium case, but still allowing to calculate all the quantities (collective velocities, temperatures, chemical potentials) necessary for estimation of the photon production. The latter, in principle, should be somewhat different from the case of chemically equilibrated evolution.

In our analysis we apply both ways of describing the evolution of hadronic system in order to compare them and get the estimation for the lower and the upper limits of the calculated direct-photon spectra and v_2 coefficients resulting from the use of such rough approximations.

In what follows we will describe how we account for the thermal photons contribution to the resulting direct-photon spectrum. However, in our study we account for the *pre-thermal* photons as well (despite the fact that, according to our estimates, their contribution to the resulting γ spectrum is only about 2% of the total thermal photon contribution), and the way we do it is quite similar to that we use for the thermal photons. The total energy-momentum tensor for the iHKM pre-thermal stage is assumed to be a sum of two parts: the hydrodynamic tensor $T^{\mu\nu}_{hydro}(x)$, multiplied by the weight $(1 - \mathcal{P}(\tau))$, and the free-streaming tensor $T^{\mu\nu}_{free}(x)$, multiplied by $\mathcal{P}(\tau)$ (see [1,2] for details). Accordingly, we treat pre-thermal photons as thermal ones, produced solely by the hydrodynamic component of the total energy-momentum tensor at the pre-thermal phase of the matter evolution, i.e., the corresponding spectrum contribution is calculated the same way as for the hydrodynamics regime, but in addition it is scaled by the factor $(1 - \mathcal{P}(\tau))$.

The momentum spectra of the thermal photons, coming from the QGP phase, can be described well already in the leading order of strong coupling constant α_s, see Reference [62].

Hence, we can use the corresponding formulas for the spectra calculations in our analysis within iHKM. The QGP thermal photon emission originates mainly from the leading order $2 \rightarrow 2$ processes (however, as it is demonstrated in [63,64], the higher-order processes can also bring noticeable contribution of parametrically the same order to the resulting spectrum of thermal photons). The photon radiation rate can be expressed by the following relativistically invariant formula

$$k^0 \frac{d^7N}{d^3\mathbf{k}d^4x} = k \cdot u \, \frac{\nu_e(k \cdot u)}{(2\pi)^3}, \tag{2}$$

where **k** is the photon momentum and **u** is the hydrodynamic velocity in the point **x**. Accordingly, the quantity $\nu_e(k \cdot u)$ can be interpreted as the spontaneous emission rate of the photons with the momentum **k**. In Reference [62] the rate $\nu_e(k \cdot u)$ was evaluated by summarizing contributions from different partonic $2 \rightarrow 2$ processes. In addition, the radiation from inelastic $q\bar{q}$ annihilation and near-collinear bremsstrahlung processes, as well as the effects of Landau–Pomeranchuk–Migdal suppression were taken into account. As a result, the total spectrum can be written as follows:

$$\frac{dN}{2\pi k_T dk_T} = \sum_i \frac{1}{(2\pi)^4} \Delta^4 V(x_i) \int_0^{2\pi} k \cdot u(x_i) \nu_e(k \cdot u(x_i)) d\phi, \tag{3}$$

where $\Delta^4 V = \tau \Delta\tau \Delta x \Delta y \Delta\eta$ is the volume of a 3D computation grid cell and the summation runs over all the grid cells, where $T > 165$ MeV, thus comprising the pre-thermal and the hydrodynamic iHKM stages. It is worth noting, that in the Formula (3) for the thermal photon spectra we neglect the corrections to the continuous Quark–Gluon matter PDFs, arising due to viscosity, since at the hydrodynamic stage of the system's expansion we assume the shear viscosity to entropy density ratio, η/s, to have the minimal possible value.

At the post-hydrodynamic (hadronic) stage of the matter evolution the same Expression (3) can be applied to estimate the thermal photon emission, however the quantity $\nu_e(k \cdot u)$ should now correspond to the radiation from hadron-resonance gas. This radiation includes many different sources that should be taken into account:

- The photons radiating from a meson gas. Here we base our consideration on the Reference [65]. We account for the hadronic reactions with π, K and ρ mesons and K^* resonances, where photons are produced. The corresponding emission rates are taken from [65] with one additional prescription for the chemically frozen evolution regime: in this case the contribution from each hadronic reaction has to be multiplied by $exp\left(\frac{\sum \mu_i(\tau,x)}{T(\tau,x)}\right)$, where $\mu_i(\tau, x)$ represent the individual chemical potentials of hadrons participating in the reaction.
- The photons coming from in-medium ρ mesons. Here we follow the results of the Reference [66]. The emission rate for these photons incorporates baryon (antibaryon) effects and in our analysis depends on the local baryon chemical potential $\mu_B(\tau, x)$ (for chemical equilibrium expansion), and, in addition, on individual chemical potentials of hadrons involved in reaction (for chemically frozen evolution).
- The photons emitted in reactions with the three mesons π, ρ and ω [19], such as $\pi\rho \rightarrow \omega\gamma$, $\pi\omega \rightarrow \rho\gamma$, and $\rho\omega \rightarrow \pi\gamma$. Again, for the chemically frozen regime the corresponding contributions should be multiplied by $exp\left(\frac{\sum \mu_i(\tau,x)}{T(\tau,x)}\right)$.
- The photons originating from $\pi\pi$ bremmstrahlung [66].

2.3. Hadronization Photons

In the work [45] an approach was developed allowing to account for the extra portion of soft photons, which presumably should be emitted from the system during the process of Quark–Gluon matter confinement (in our study within iHKM it corresponds to an extra γ emission at the particlization phase of the system's evolution). Such additional electromagnetic radiation could take place, e.g., via the mechanism of "magnetic bremsstrahlung-like" (synchrotron) radiation, coming from the interaction of quarks, which escape from QGP, with the confining collective color field [40]. Other possible mechanisms of additional photon emission are considered in the papers [41–44,67]. Despite some of these mechanisms can improve calculated direct-photon spectra significantly, the corresponding models are still phenomenological and incomplete, since the considered processes are non-perturbative and non-equilibrium. In order to avoid uncertainties associated with the use of different theoretical models and their different calibration, in our approach we aim to implement the mechanism of confinement emission in a simplest phenomenological way possible.

Let us introduce the emission function of extra photon radiation at the particlization (hadronization) stage, $G_{hadr}(t, \mathbf{r}, p)$, as follows:

$$\frac{d^3N_\gamma}{d^3p} = \int dt d^3r \, G_{hadr}(t, \mathbf{r}, p). \tag{4}$$

Then let us also consider the hypersurface of maximal emission for the photons possessing 4-momentum p. For each given p such a hypersurface σ can be constructed as a set of corresponding space-time points $(t_\sigma, \mathbf{r})$, where $t_\sigma = t_\sigma(\mathbf{r}, p)$. Following the recipe utilized in [68,69], one can switch to new space coordinates $\mathbf{x} = \mathbf{r} + \frac{\mathbf{p}}{p^0} t_\sigma(\mathbf{r}, p)$, including the saddle point $t_\sigma(\mathbf{r}, p)$. The emission function $G_{hadr}(t, \mathbf{x}, p)$ after that can be approximately presented (using saddle point method) as $G_{hadr} \approx F(t, \mathbf{x}, p) \exp(-\frac{(t-t_\sigma)^2}{2D^2})$, where F should be a function, depending smoothly on time t. The application of such an approximation gives one the following spectrum:

$$\frac{d^3N_\gamma}{d^3p} = \int d^3x \left| 1 - \frac{\mathbf{p}}{p^0} \frac{\partial t_\sigma(\mathbf{x}, p)}{\partial \mathbf{x}} \right| \int dt F(t_\sigma(\mathbf{x}, p), \mathbf{x}, p) \exp\left(- \frac{(t - t_\sigma(\mathbf{x}, p))^2}{2D_c^2(t_\sigma(\mathbf{x}, p), \mathbf{x}, p)} \right). \tag{5}$$

If we then assume that the considered hypersurface of maximal emission coincides for soft photons with the common hypersurface of hadronization (in iHKM we use the isotherm $T_h = 165$ MeV as such hadronization hypersurface), the previous equation can be rewritten as follows:

$$p^0 \frac{d^3N_\gamma}{d^3p} = \int_{\sigma_h} d^3\sigma_\mu(x) p^\mu F(p \cdot u(x), T_h) D_c(p \cdot u(x), T_h) \theta(d\sigma_\mu(x) p^\mu), \tag{6}$$

where the chemical potentials at $T = T_h$ are assumed to be vanishing in case of the LHC high-energy collisions, and the Heaviside function $\theta(x)$ is introduced to cut off possible negative contributions to the momentum spectra from non-space-like pieces of the particlization hypersurface. Note, that the quantity D_c (representing the emission temporal width in the obtained Expression (6) for momentum spectra) is assumed to depend on collision centrality c, reflecting the fact that the created fireball expands and hadronizes faster for non-central collisions due to higher gradients in transverse direction, caused by smaller transverse size of the system in this case.

Let us further assume, following the work [44] and our articles [45,46], that the photon emission function, approximated in our consideration by the product of the two functions $F \cdot D_c$, can be presented in the following thermal-like form:

$$F(p \cdot u(x), T_h) \cdot D_c(p \cdot u(x), T_h) = \gamma_{hadr} d_c f_\gamma^{eq}(p \cdot u(x), T_h) \tag{7}$$

$$= \gamma_{hadr} d_c \frac{1}{(2\pi)^3} \frac{g}{\exp(p \cdot u(x)/T_h) - 1}, \tag{8}$$

with the factor $g = 2$.

The quantity γ_{hadr} in the above formula characterizes the QGP confinement process itself (its basic properties), while the parameter $d_c \propto \langle D \rangle$ characterizes its temporal width and thus can be possibly different for different centrality classes. However, in our analysis, carried out in the References [45,46], we combined the product of these two parameters, γ_{hadr} and d_c, into a single parameter $\beta \equiv d_c \gamma_{hadr}$ and used the same its value to describe the hadronization emission of photons for all the considered centrality classes at given collision energy. The value $\beta = 0.04$ was used in the case of Au+Au collisions at the top RHIC energy [46] and the value $\beta = 0.02$ was used even earlier for 2.76A TeV Pb+Pb collisions at the LHC [45]. Note, however, that the photon momentum spectra measured by the STAR Collaboration at RHIC [70] can also be described in iHKM with the "LHC value", $\beta = 0.02$, and re-tuning to $\beta = 0.04$ is necessary to describe at the same time the data on elliptic and triangular flows, measured by the PHENIX Collaboration [71].

The possible reason for the observed distinction between the β values used for RHIC and for LHC can be connected with the corresponding difference between the maximal intensities of the hadronization process at the two colliders. The hadronization intensity most likely should be smaller at the LHC, because of much higher system's expansion rate in this case, which would impede the quark coalescence. The detailed study of the interplay between different factors affecting the β parameter value is, however, outside the scope of current paper and can be carried out in further works.

3. Results and Discussion

In the papers [45,46] to describe the photon production at RHIC and the LHC we utilized the same model parameters tuning which previously ensured the successful description of hadron observables at the same collision energies [5,6]. As a result of analysis carried out in [45,46] it was found that the description of direct-photon p_T spectra, elliptic and triangular flow p_T-dependencies, $v_2(p_T)$ and $v_3(p_T)$, can be significantly improved, for both RHIC and the LHC energies, if one includes, along with the contributions from prompt, pre-thermal and thermal (QGP and hadron gas) photon emission, an additional portion of γ radiation, corresponding to the confinement process, which can be called the "hadronization photons" (see Figure 1, demonstrating the RHIC and the LHC photon spectra calculated within the iHKM for the central events (c = 0–20%); the spectra obtained with and without accounting for the hadronization emission (HE) are shown). Comparing the model spectra for the two simulation modes with the experimental points presented by the PHENIX [25] and the ALICE [28] Collaborations, we can definitely say that for both collision energies the inclusion of the HE component makes the simulation results much closer to the measured data.

In iHKM the magnitude of the HE contribution is regulated by the only one free parameter β, which characterizes the intensity of the photon emission during the process of confinement. In order to fix the value of the β parameter, one should at first perform fitting of the direct-photon spectrum for the case of most central events. Having determined in such a way the value of the HE parameter, one can further use it for all the centrality classes for the description of transverse momentum photon spectra, together with elliptic and triangular flows. Our analysis gives the value $\beta = 0.02$ for the LHC Pb+Pb collisions at the energy 2.76A TeV and the value $\beta = 0.04$ for the RHIC Au+Au collisions at 200A GeV.

As for the dependence of the simulation results on the variant of the matter evolution treatment at the afterburner stage of the collision (chemically equilibrated vs. chemically frozen evolution), the photon p_T spectra corresponding to these two approaches are compared in Figure 2. From the plot one can conclude, that both calculation regimes give very close results, although the chemically frozen evolution leads to hardly noticeable lowering of the total spectra. The same concerns the results for elliptic flow coefficients v_2.

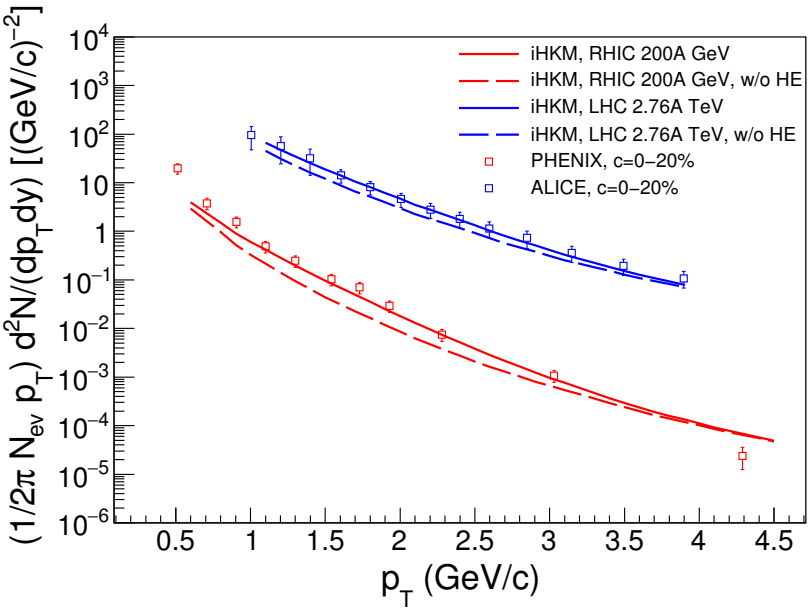

Figure 1. The photon spectra calculated within the iHKM for the RHIC 200A GeV and the LHC 2.76A TeV A+A collisions, in comparison with the corresponding experimental data [25,28]. The events from the centrality class c = 0–20% are analyzed. The solid lines are related to the simulations where the hadronization emission is taken into account, while the dashed lines represent the simulations where HE was ignored.

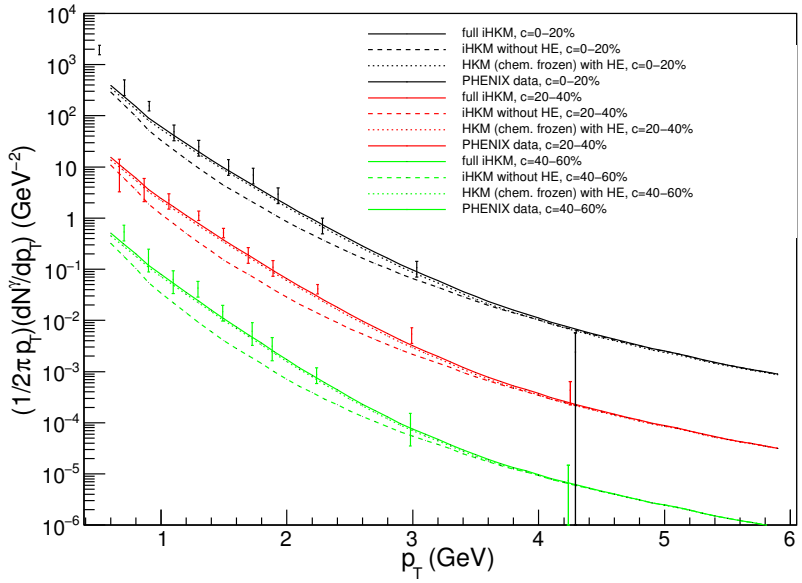

Figure 2. The total direct-photon p_T spectra in the top RHIC energy Au+Au collisions, obtained by the summation of the different sets of components: the photon radiation calculated within the iHKM with chemically equilibrated evolution at the final stage of the expansion and with the Hadronization Emission (HE) contribution taken into account; the same as in previous case, but without the HE contribution; the photon radiation from the HKM with the chemically frozen evolution at the hadronic stage together with the contribution from the HE. The results for the three centrality classes, c = 0–20%, c = 20–40%, and c = 40–60% are shown. The spectra for the c = 0–20% centrality class are multiplied by 100, and the spectra for c = 20–40% are multiplied by 10. The experimental points are taken from [25].

So, despite our assumption that changing the approach to the description of the system's post-hydrodynamic expansion should in theory lead to changes in the resulting photon spectra, we see that on practice the difference is fairly insignificant. One can explain such a result by mutual compensation of particular changes brought to the model simulation by switching to another matter evolution treatment. Specifically, the emergence of additional hadron chemical potentials, which accompanies our passage to the chemically frozen evolution scenario, could be compensated by a simultaneous lowering of the temperatures, associated with certain energy density values. The latter lowering, in turn, could happen due to interplay between the changes in the system's expansion rate and in its chemical composition, taking place when one switches from the chemically equilibrated to the chemically frozen regime (see [61,68]).

An interesting detail concerning the dependency of the total direct-photon yield on the mean charged-particle multiplicity $\langle \frac{dN_{ch}}{d\eta} \rangle$ (see Table 1) seems to be worth noting: in our model calculations we obtained that the total yield of soft direct photons is approximately proportional to $\langle \frac{dN_{ch}}{d\eta} \rangle^{1.25}$ [46]. This feature of the iHKM results is in agreement with the results of experimental measurements of the PHENIX Collaboration [72]. From Table 1 one can also see that for all the centralities the magnitude of the contribution from the hadronization emission photons to the total yield is comparable with that of the thermal photon contribution (which includes the emission from both QGP and hadron matter phases), while the contribution of prompt photons is about two-times smaller. The thermal and hadronization photons, however, dominate only in a relatively-low-momentum region, $p_T < 3$ GeV/c, while for high $p_T > 3 - 4$ GeV/c prompt photon emission gives the main contribution to the total spectrum (see Figure 1 from [45] and Figure 4 from [46]).

Table 1. The different contributions to the total direct-photon yield in iHKM for the top RHIC energy Au+Au collisions. The data for the three collision centrality classes together with the corresponding mean charged particle multiplicities $\langle \frac{dN_{ch}}{d\eta} \rangle$ are presented.

Centrality, %	$\langle \frac{dN_{ch}}{d\eta} \rangle$	**Prompt** γ	**Thermal** γ	**Hadroniz.** γ	**Total** γ	$a \cdot \langle \frac{dN_{ch}}{d\eta} \rangle^{1.25}$
0–20	567	0.2471	0.5000	0.5499	1.2970	1.2970
20–40	236	0.0905	0.1727	0.2314	0.4946	0.4337
40–60	98	0.0265	0.0456	0.0751	0.1472	0.1446

One can also see our results on direct-photon $v_2(p_T)$ and $v_3(p_T)$ dependencies, obtained in iHKM for the Au+Au collisions at the top RHIC energy, c = 20–40%, in Figure 3. The experimental points reported by the PHENIX Collaboration [71] are shown as well for comparison purposes. Again, we see that the hadronization photons play an important role in bettering the description of the experimental data within the model. This, in particular, should imply that the expanding matter situated in a thin space-time layer enclosing the hadronization hypersurface is strongly involved into collective motion. Comparing the results on flow harmonics for different collision centralities (see Figures 6–11 from the paper [46]) one can also conclude that the relative contribution of the hadronization emission to v_n values increases when one passes from central events to peripheral ones.

In Figure 4 we also show the results on $v_2(p_T)$ dependency for the LHC energy 2.76A TeV. In addition to the curves presented for RHIC we include here the elliptic flow coefficients calculated in iHKM for the thermal photons only (excluding the contributions from prompt and hadronization photons). The corresponding curve goes even higher and closer to the experimental data than the curve for the full iHKM calculation with the HE contribution. Such a peculiarity can be explained if one notices that the prompt photon radiation is momentum isotropic, so that its inclusion into resulting v_2 coefficients suppresses the anisotropy, specific for the thermal photon momentum spectra. This effect manifests itself the stronger, the more peripheral collision events we consider [45].

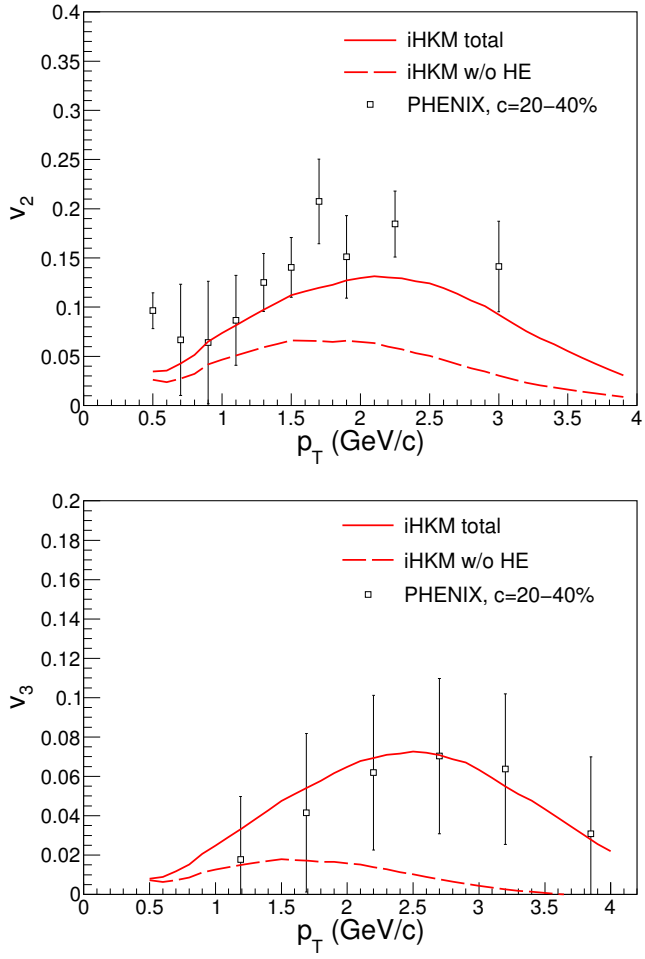

Figure 3. The photon $v_2(p_T)$ and $v_3(p_T)$ flow harmonics behavior calculated in iHKM for the case of the top RHIC energy Au+Au collisions with the centrality c = 20–40% in comparison with the measured experimental data [71]. The solid lines are related to the simulations where the hadronization emission is taken into account, while the dashed lines represent the simulations where HE was ignored.

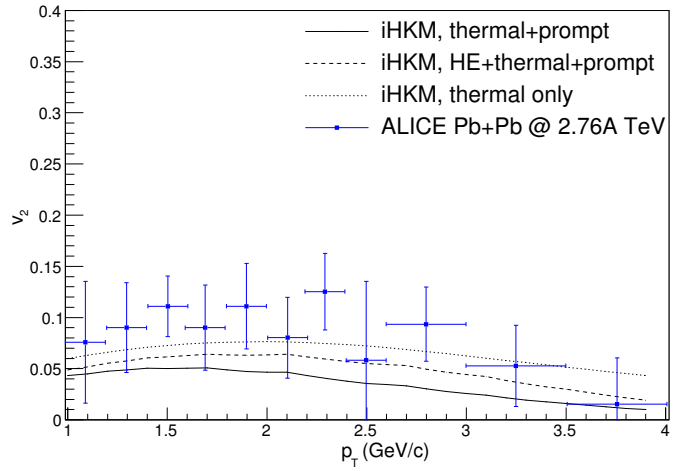

Figure 4. The dependency of the photon v_2 coefficients on p_T calculated in iHKM for the case of the LHC Pb+Pb collisions at $\sqrt{s_{NN}}$ = 2.76 TeV with the centrality c = 0–40% in comparison with the measured experimental data [73]. The results obtained with and without taking into account the hadronization emission are demonstrated, as well as the results including only thermal photon component (without prompt photon contribution).

4. Conclusions

The previously obtained results on direct-photon yields, momentum spectra, v_2 and v_3 flow harmonics obtained within the integrated hydrokinetic model of relativistic nucleus-nucleus collisions for the top RHIC energy 200A GeV and the LHC energy 2.76A TeV are summarized and reviewed.

The comparison of the chemically equilibrated and the chemically frozen descriptions of the matter evolution at the post-hadronization stage shows that the chemically frozen expansion treatment leads to a slightly lower resulting p_T spectra and v_n coefficients of direct photons.

The main conclusion that can be drawn from the performed analysis is that the problem of simultaneous theoretical description of the direct-photon spectra and flow harmonics, which appear to have unexpectedly large values in the experimental data, referred to as the "direct photon flow puzzle", probably can be solved if one accounts for the extra contribution to the photon production connected with the process of confinement (hadronization) in the considered strongly interacting system. The most simple phenomenological accounting for this additional portion of radiation is sufficient to significantly improve the agreement between the model and experimental results.

A satisfactory photon data description was obtained within the iHKM using the same basic model parameters tuning, which was used earlier for the description of hadronic observables at the considered collision energies. The elucidated dynamics creates a reliable basis for the study of other phenomena and also mechanisms of the production of exotic particles, e.g., those containing heavy flavors.

Author Contributions: Conceptualization, Y.S.; data curation, V.S.; funding acquisition, Y.S.; methodology, Y.S.; project administration, Y.S.; supervision, Y.S.; visualization, V.S.; writing—original draft, V.S.; writing—review and editing, V.S. and Y.S. All authors have read and agreed to the published version of the manuscript.

Funding: The research was carried out within the NAS of Ukraine Targeted research program "Collaboration in advanced international projects on high-energy physics and nuclear physics", Agreement 7-2022 between the NAS of Ukraine and BITP of the NAS of Ukraine.

Conflicts of Interest: The authors declare no conflict of interest. The funders had no role in the design of the study; in the collection, analyses, or interpretation of data; in the writing of the manuscript, or in the decision to publish the results.

References

1. Naboka, V.Y.; Akkelin, S.V.; Karpenko, I.A.; Sinyukov, Y.M. Initialization of hydrodynamics in relativistic heavy ion collisions with an energy-momentum transport model. *Phys. Rev. C* **2015**, *91*, 014906. [CrossRef]
2. Naboka, V.Y.; Karpenko, I.A.; Sinyukov, Y.M. Thermalization, evolution, and observables at energies available at the CERN Large Hadron Collider in an integrated hydrokinetic model of A+A collisions. *Phys. Rev. C* **2016**, *93*, 024902. [CrossRef]
3. Shapoval, V.M.; Braun-Munzinger, P.; Sinyukov, Y.M. $K^*(892)$ and $\phi(1020)$ production and their decay into the hadronic medium at the Large Hadron Collider. *Nucl. Phys. A* **2017**, *968*, 391. [CrossRef]
4. Sinyukov, Y.M.; Shapoval, V.M. Particle production at energies available at the CERN Large Hadron Collider within evolutionary model. *Phys. Rev. C* **2018**, *97*, 064901. [CrossRef]
5. Shapoval, V.M.; Sinyukov, Y.M. Bulk observables in Pb+Pb collisions at $\sqrt{s_{NN}} = 5.02$ TeV at the CERN Large Hadron Collider within the integrated hydrokinetic model. *Phys. Rev. C* **2019**, *100*, 044905. [CrossRef]
6. Adzhymambetov, M.D.; Shapoval, V.M.; Sinyukov, Y.M. Description of bulk observables in Au+Au collisions at top RHIC energy in the integrated hydrokinetic model. *Nucl. Phys. A* **2019**, *987*, 321. [CrossRef]
7. Sinyukov, Y.; Adzhymambetov, M.; Shapoval, V. Particle Production in Xe+Xe Collisions at the LHC within the Integrated Hydrokinetic Model. *Particles* **2020**, *3*, 114. [CrossRef]
8. Feinberg, E.L. Perturbative approach to some one-dimensional many-body problems. I: Discussion of the Rayleigh-Schrödinger and Brillouin-Wigner series for the Sutherland model. *Il Nuovo Cimento B* **1976**, *34*, 391.
9. Shuryak, E.V. Quark-Gluon Plasma and Hadronic Production of Leptons, Photons and Psions. *Sov. J. Nucl. Phys.* **1978**, *28*, 408. [CrossRef]
10. Ruuskanen, P.V. Electromagnetic probes of quark-gluon plasma in relativistic heavy-ion collisions. *Nucl. Phys. A* **1992**, *544*, 169. [CrossRef]
11. Thoma, M.H. Damping rate of a hard photon in a relativistic plasma. *Phys. Rev. D* **1995**, *51*, 862. [CrossRef]

12. Roy, P.; Sarkar, S.; Alam, J.; Sinha, B. Electromagnetic radiation from hot and dense hadronic matter. *Nucl. Phys. A* **1999**, *653*, 277. [CrossRef]
13. Paquet, J.-F.; Shen, C.; Denicol, G.S.; Luzum, M.; Schenke, B.; Jeon, S.; Gale, C. Production of photons in relativistic heavy-ion collisions. *Phys. Rev. C* **2016**, *93*, 044906. [CrossRef]
14. Berges, J.; Reygers, K.; Tanji, N.; Venugopalan, R. Parametric estimate of the relative photon yields from the glasma and the quark-gluon plasma in heavy-ion collisions. *Phys. Rev. C* **2017**, *95*, 054904. [CrossRef]
15. Chiu, M.; Hemmick, T.K.; Khachatryan, V.; Leonidov, A.; Liao, J.; McLerran, L. Production of Photons and Dileptons in the Glasma. *Nucl. Phys. A* **2013**, *900*, 16. [CrossRef]
16. van Hees, H.; Gale, C.; Rapp, R. Thermal photons and collective flow at energies available at the BNL Relativistic Heavy-Ion Collider. *Phys. Rev. C* **2011**, *84*, 054906. [CrossRef]
17. Rapp, R.; van Hees, H.; He, M. Properties of thermal photons at RHIC and LHC. *Nucl. Phys. A* **2014**, *931*, 696. [CrossRef]
18. Gale, C. Photon production in hot and dense strongly interacting matter, in: Landolt–Bornstein—Group I Elementary Particles, Nuclei and Atoms. *Relativ. Heavy Ion Phys.* **2010**, *23*, 445.
19. Holt, N.P.M.; Hohler, P.M.; Rapp, R. Thermal photon emission from the $\pi\rho\omega$ system. *Nucl. Phys. A* **2016**, *945*, 1. [CrossRef]
20. Fries, R.J.; Muller, B.; Srivastava, D.K. High-Energy Photons from Passage of Jets through Quark-Gluon Plasma. *Phys. Rev. Lett.* **2003**, *90*, 132301. [CrossRef]
21. Turbide, S.; Gale, C.; Frodermann, E.; Heinz, U. Electromagnetic radiation from nuclear collisions at ultrarelativistic energies. *Phys. Rev. C* **2008**, *77*, 024909. [CrossRef]
22. Adare, A; Afanasiev, S.; Aidala, C.; Ajitanand, N.N.; Akiba, Y.; Al-Bataineh, H.; Alexander, J.; Al-Jamel, A.; Aoki, K.; Aphecetche, L.; et al. Enhanced Production of Direct Photons in Au+Au Collisions at $\sqrt{s_{NN}} = 200$ GeV and Implications for the Initial Temperature. *Phys. Rev. Lett.* **2010**, *104*, 132301. [CrossRef] [PubMed]
23. Adare, A; Afanasiev, S.; Aidala, C.; Ajitanand, N.N.; Akiba, Y.; Al-Bataineh, H.; Alexander, J.; Aoki, K.; Aramaki, Y.; Atomssa, E.T.; et al. Observation of Direct-Photon Collective Flow in Au+Au Collisions at $\sqrt{s_{NN}} = 200$ GeV. *Phys. Rev. Lett.* **2012**, *109*, 122302. [CrossRef]
24. Adare, A; Afanasiev, S.; Aidala, C.; Ajitanand, N.N.; Akiba, Y.; Al-Bataineh, H.; Alexander, J.; Al-Jamel, A.; Aoki, K.; Aphecetche, L.; et al. Detailed measurement of the e^+e^- pair continuum in p+p and Au+Au collisions at $\sqrt{s_{NN}} = 200$ GeV and implications for direct photon production. *Phys. Rev. C* **2010**, *81*, 034911. [CrossRef]
25. Adare, A; Afanasiev, S.; Aidala, C.; Ajitanand, N.N.; Akiba, Y.; Akimoto, R.; Al-Bataineh, H.; Al-Ta'ani, H.; Alexander, J.; Angerami, A.; et al. Centrality dependence of low-momentum direct-photon production in Au+Au collisions at $\sqrt{s_{NN}} = 200$ GeV. *Phys. Rev. C* **2015**, *91*, 064904. [CrossRef]
26. Wilde, M.; ALICE Collaboration. Measurement of Direct Photons in pp and Pb-Pb Collisions with ALICE. *Nucl. Phys. A* **2013**, *904*, 573c. [CrossRef]
27. Lohner, D.; ALICE Collaboration. Measurement of Direct-Photon Elliptic Flow in Pb-Pb Collisions at $\sqrt{s_{NN}} = 2.76$ TeV. *J. Phys. Conf. Ser.* **2013**, *446*, 012028. [CrossRef]
28. Adam, J.; Adamová, D.; Aggarwal, M.M.; Aglieri Rinella, G.; Agnello, M.; Agrawal, N.; Ahammed, Z.; Ahn, S.U.; Aiola, S.; Akindinov, A.; et al. Direct photon production in Pb–Pb collisions at $\sqrt{s_{NN}} = 2.76$ TeV. *Phys. Lett. B* **2016**, *754*, 235.
29. Holopainen, H.; Räsänen, S.S.; Eskola, K.J. Elliptic flow of thermal photons in heavy-ion collisions at energies available at the BNL Relativistic Heavy Ion Collider and at the CERN Large Hadron Collider. *Phys. Rev. C* **2011**, *84*, 064903. [CrossRef]
30. Chaudhuri, A.K.; Sinha, B. Direct photon production from viscous quark-gluon plasma. *Phys. Rev. C* **2011**, *83*, 034905. [CrossRef]
31. Shen, C.; Heinz, U.; Paquet, J.-F.; Gale, C. Thermal photons as a quark-gluon plasma thermometer reexamined. *Phys. Rev. C* **2014**, *89*, 044910. [CrossRef]
32. Liu, F.-M.; Liu, S.-X. Quark-gluon plasma formation time and direct photons from heavy ion collisions. *Phys. Rev. C* **2014**, *89*, 034906. [CrossRef]
33. Chatterjee, R.; Holopainen, H.; Helenius, I.; Renk, T.; Eskola, K.J. Elliptic flow of thermal photons from an event-by-event hydrodynamic model. *Phys. Rev. C* **2013**, *88*, 034901. [CrossRef]
34. Chatterjee, R.; Srivastava, D.K.; Renk, T. Triangular flow of thermal photons from an event-by-event hydrodynamic model for 2.76*A* TeV Pb+Pb collisions at the CERN Large Hadron Collider. *Phys. Rev. C* **2016**, *94*, 014903. [CrossRef]
35. Kim, Y.-M.; Lee, C.-H.; Teaney, D.; Zahed, I. Direct photon elliptic flow at energies available at the BNL Relativistic Heavy Ion Collider and the CERN Large Hadron Collider. *Phys. Rev. C* **2017**, *96*, 015201. [CrossRef]
36. Basar, G.; Kharzeev, D.E.; Skokov, V. Conformal Anomaly as a Source of Soft Photons in Heavy Ion Collisions. *Phys. Rev. Lett.* **2012**, *109*, 202303. [CrossRef]
37. Müller, B.; Wu, S.-Y.; Yang, D.-L. Elliptic flow from thermal photons with magnetic field in holography. *Phys. Rev. D* **2014**, *89*, 026013. [CrossRef]
38. Zakharov, B. Induced photon emission from quark jets in ultrarelativistic heavy-ion collisions. *JETP Lett.* **2014**, *80*, 1. [CrossRef]
39. Tuchin, K. Role of magnetic field in photon excess in heavy ion collisions. *Phys. Rev. C* **2015**, *91*, 014902. [CrossRef]
40. Goloviznin, V.V.; Snigirev, A.M.; Zinovjev, G.M. Towards azimuthal anisotropy of direct photons. *JETP Lett.* **2013**, *98*, 61. [CrossRef]
41. Kharzeev, D.E.; Loshaj, F. Anomalous soft photon production from the induced currents in Dirac sea. *Phys. Rev. D* **2014**, *89*, 074053. [CrossRef]

42. Campbell, S. Photon production from gluon-mediated quark–anti-quark annihilation at confinement. *Phys. Rev. C* **2015**, *92*, 014907. [CrossRef]
43. Young, C.; Pratt, S. Electromagnetic recombination spectra at the quark-hadron phase transition. *Phys. Rev. C* **2016**, *94*, 044916. [CrossRef]
44. Fujii, H.; Itakura, K.; Nonaka, C. Photon emission at hadronization. *Nucl. Phys. A* **2017**, *967*, 704. [CrossRef]
45. Naboka, V.Y.; Sinyukov, Y.M.; Zinovjev, G.M. Direct-photon spectrum and elliptic flow produced from Pb+Pb collisions at $\sqrt{s_{NN}} = 2.76$ TeV at the CERN Large Hadron Collider within an integrated hydrokinetic model. *Phys. Rev. C* **2018**, *97*, 054907. [CrossRef]
46. Naboka, V.Y.; Sinyukov, Y.M.; Zinovjev, G.M. Photon spectra and anisotropic flow in heavy ion collisions at the top RHIC energy within the integrated hydrokinetic model with photon hadronization emission. *Nucl. Phys. A* **2020**, *1000*, 121843. [CrossRef]
47. Aad, G.; Abbott, B.; Abdallah, J.; Abdel Khalek, S.; Abdinov, O.; Aben, R.; Abi, B.; Abolins, M.; AbouZeid, O.S.; Abramowicz, H.; et al. Centrality, rapidity, and transverse momentum dependence of isolated prompt photon production in lead-lead collisions at $\sqrt{s_{NN}} = 2.76$ TeV measured with the ATLAS detector. *Phys. Rev. C* **2016**, *93*, 034914. [CrossRef]
48. Chatrchyan, S.; Khachatryan, V.; Sirunyan, A.M.; Tumasyan, A.; Adam, W.; Bergauer, T.; Dragicevic, M.; Erö, J.; Fabjan, C.; Friedl, M.; et al. Measurement of isolated photon production in pp and PbPb collisions at $\sqrt{s_{NN}} = 2.76$ TeV. *Phys. Lett. B* **2012**, *710*, 256. [CrossRef]
49. Abelev, B.; Adam, J.; Adamová, D.; Adare, A.M.; Aggarwal, M.M.; Aglieri Rinella, G.; Agnello, M.; Agocs, A.G.; Agostinelli, A.; Ahammed, Z.; et al. Centrality determination of Pb-Pb collisions at $\sqrt{s_{NN}} = 2.76$ TeV with ALICE. *Phys. Rev. C* **2013**, *88*, 044909. [CrossRef]
50. Aurenche, P.; Guillet, J.P.; Pilon, E.; Werlen, M.; Fontannaz, M. Recent critical study of photon production in hadronic collisions. *Phys. Rev. D* **2006**, *73*, 094007. [CrossRef]
51. Eskola, K.; Paukkunen, H.; Salgado, C. EPS09—A new generation of NLO and LO nuclear parton distribution functions. *J. High Energy Phys.* **2009**, *4*, 065. [CrossRef]
52. Bourhis, L.; Fontannaz, M.; Guillet, J.P. Quark and gluon fragmentation functions into photons. *Eur. Phys. J. C* **1998**, *2*, 529. [CrossRef]
53. Akkelin, S.V.; Sinyukov, Y.M. Matching of nonthermal initial conditions and hydrodynamic stage in ultrarelativistic heavy-ion collisions. *Phys. Rev. C* **2010**, *81*, 064901. [CrossRef]
54. Broniowski, W.; Rybczynski, M.; Bozek, P. GLISSANDO: GLauber Initial-State Simulation AND mOre. *Comput. Phys. Commun.* **2009**, *180*, 69. [CrossRef]
55. Rybczynski, M.; Stefanek, G.; Broniowski, W.; Bozek, P. GLISSANDO 2: GLauber Initial-State Simulation AND mOre..., ver. 2. *Comput. Phys. Commun.* **2014**, *185*, 1759. [CrossRef]
56. Bozek, P.; Broniowski, W.; Rybczynski, M.; Stefanek, G. GLISSANDO 3: GLauber Initial-State Simulation AND mOre..., ver. 3. *Comput. Phys. Commun.* **2019**, *245*, 106850. [CrossRef]
57. Laine, M.; Schroeder, Y. Quark mass thresholds in QCD thermodynamics *Phys. Rev. D* **2006**, *73*, 085009. [CrossRef]
58. Huovinen, P.; Petersen, H. Particlization in hybrid models. *Eur. Phys. J. A* **2012**, *48*, 171. [CrossRef]
59. Bass, S.A.; Belkacem, M.; Bleicher, M.; Brandstetter, M.; Bravina, L.; Ernst, C.; Gerland, L.; Hofmann, M.; Hofmann, S.; Konopka J.; et al. Microscopic Models for Ultrarelativistic Heavy Ion Collisions. *Prog. Part. Nucl. Phys.* **1998**, *41*, 225. [CrossRef]
60. Bleicher, M.; Zabrodin, E.; Spieles, C.; Bass, S.A.; Ernst, C.; Soff, S.; Bravina, L.; Belkacem, M.; Weber, H.; Stocker H.; et al. Relativistic Hadron-Hadron Collisions in the Ultra-Relativistic Quantum Molecular Dynamics Model. *J. Phys. G Nucl. Part. Phys.* **1999**, *25*, 1859. [CrossRef]
61. Karpenko, I.A.; Sinyukov, Y.M. Kaon and pion femtoscopy at the highest energies available at the BNL Relativistic Heavy Ion Collider (RHIC) in a hydrokinetic model. *Phys. Rev. C* **2010**, *81*, 054903. [CrossRef]
62. Arnold, P.B.; Moore, G.D.; Yaffe, L.G. Photon emission from quark-gluon plasma: complete leading order results. *J. High Energy Phys.* **2001**, *12*, 009. [CrossRef]
63. Aurenche, P.; Gelis, F.; Zaraket, H. Kinoshita-Lee-Nauenberg theorem, magnetic mass, and thermal photon production. *Phys. Rev. D* **2000**, *61*, 116001. [CrossRef]
64. Ghiglieri, J.; Hong, J.; Kurkela, A.; Lu, E.; Moore, G.D.; Teaney, D. Next-to-leading order thermal photon production in a weakly coupled quark-gluon plasma. *J. High Energy Phys.* **2013**, *5*, 010. [CrossRef]
65. Turbide, S.; Rapp, R.; Gale, C. Hadronic production of thermal photons. *Phys. Rev. C* **2004**, *69*, 014903. [CrossRef]
66. Heffernan, M.; Hohler, P.; Rapp, R. Universal parametrization of thermal photon rates in hadronic matter. *Phys. Rev. C* **2015**, *91*, 027902. [CrossRef]
67. Nayak, G.C. Parton to Hadron Fragmentation Function from Quark-Gluon Plasma using Lattice QCD Method at Finite Temperature. *arXiv* **2019**, arXiv:1904.05376.
68. Akkelin, S.V.; Hama, Y.; Karpenko, I.A.; Sinyukov, Y.M. Hydro-kinetic approach to relativistic heavy ion collisions. *Phys. Rev. C* **2008**, *78*, 034906. [CrossRef]
69. Sinyukov, Y.M.; Akkelin, S.V.; Karpenko, I.A. Kinetics Versus Hydrodynamics: Generalization of Landau/Cooper–Frye Prescription for Freeze-Out. *Act. Phys. Pol. B* **2009**, *40*, 1025.

70. Adamczyk, L.; Adkins, J.K.; Agakishiev, G.; Aggarwal, M.M.; Ahammed, Z.; Ajitanand, N.N.; Alekseev, I.; Anderson, D.M.; Aoyama, R.; Aparin, A.; et al. Direct virtual photon production in Au+Au collisions at $\sqrt{s_{NN}} = 200$ GeV. *Phys. Lett. B* **2017**, *770*, 451. [CrossRef]
71. Adare, A; Afanasiev, S.; Aidala, C.; Ajitanand, N.N.; Akiba, Y.; Akimoto, R.; Al-Bataineh, H.; Alexander, J.; Alfred, M.; Al-Ta'ani, H.; et al. Azimuthally anisotropic emission of low-momentum direct photons in Au+Au collisions at $\sqrt{s_{NN}} = 200$ GeV. *Phys. Rev. C* **2016**, *94*, 064901. [CrossRef]
72. Roman, V.C.; PHENIX Collaboration. Direct Photons at the PHENIX Experiment: From Large to Small Systems. *Proceedings* **2019**, *10*, 32. [CrossRef]
73. Lohner, D. Anisotropic flow of direct photons in Pb-Pb collisions at 2.76 TeV per nucleon. Ph.D. Thesis, University of Heidelberg, Heidelberg, Germany, 2013.